Biosensors and Bioelectronics 109 (2018) 237–245

Contents lists available at ScienceDirect

Biosensors and Bioelectronics

journal homepage: www.elsevier.com/locate/bios

One-step selective screening of bioactive molecules in living cells using sulfur-doped microporous carbon

Mohammed Y. Emran[a], Mohamed A. Shenashen[a], Hiromi Morita[b], Sherif A. El-Safty[a,c,*]

[a] Center for Functional Materials, National Institute for Materials Science (NIMS), 1-2-1 Sengen, Tsukuba-shi, Ibaraki-ken 305-0047, Japan
[b] Nanotechnology Innovation Station, National Institute for Materials Science (NIMS), 1-2-1 Sengen, Tsukuba 305-0047, Japan
[c] Faculty of Engineering and Advanced Manufacturing, University of Sunderland, St Peter's Campus, Sunderland SR6 0DD, UK

ARTICLE INFO

Keywords:
Extracellular DA
Biological samples
Biosensor
Mono-bioactive molecules
Living cells
Biocompatibility and low cytotoxicity

ABSTRACT

A metal-free electrode using heteroatom-doped microporous carbon was fabricated for the ultrasensitive monitoring of mono-bioactive molecules and the selective signaling of dopamine (DA) secreted by living cells. The constructed electrode based on sulfur-doped microporous carbon (S-MC) shows a high surface area, a spherical construction, numerous carbon chain defects, and microporous structures, which are the key factors of the interactive signaling transducer, fast response, and active interfacial surfaces. The intrinsic features of S-MC with different %S-doping (S-MC-1, and S-MC-2) through the sp^2-carbon chain create abundant catalytic active sites, facilitate molecular diffusion through the microporous structure, promote strong binding with the targeted molecules, and induce interactions at electrolyte–electrode interfaces. The S-MC-1 provides selective signaling in a tertiary mixture of DA, ascorbic acid (AA), and uric acid (UA) with a high sensitivity and a wide linear range of 0.01–5, 10–4000, and 1–2000 μM, respectively. The detection limits were set at 3 nM, 1.26 μM, and 0.23 μM for DA, AA, and UA respectively. The S-MC-1 demonstrated a selective screening of DA released from PC12 cells under a K^+ ion- stimulator with high sensitivity and promoted high biocompatibility, low cytotoxicity, high stability, and reliable reproducibility (%RSD ranged from 1 to 2.7). Our findings indicated that the S-MC-1 can be utilized as an in-vitro model for simultaneously monitoring extracellular-DA secreted from living cells and sensing mono-bioactive molecules in biological samples.

1. Introduction

The control and early investigation of various diseases and genetic problems depend on the level of bioactive molecules, such as dopamine (DA), ascorbic acid (AA), and uric acid (UA), (Chen and Chatterjee, 2013; Li et al., 2013). For instance, DA is a catecholamine neurotransmitter in the mammalian central nervous system, where it controls learning, cognition, locomotion, emotion, and working memory (Zhang et al., 2015a). The investigation of neurological disorders and psychiatric disturbances, such as schizophrenia, cocaine addiction, and Parkinson's disease is depended on the DA level in the brain and/or human blood serum (Farjami et al., 2012; Zhang et al., 2015a). The AA target may act as antioxidants in the human diet, leading to play an important role in the prevention and treatment of several diseases, such as the common cold, mental illnesses, scurvy, and AIDS, as reported elsewhere (Huang et al., 2008). UA is one of the mono molecules present in human fluids, and its level in urine and serum is an indicator of several diseases, such as gout, hyperuricemia, and Lesch-Nyhan syndrome (Jiang and Du, 2014). The successful development of a biosensor for the rapid, cost-effective, and on-site monitoring of a wide linear range of targets is gaining considerable interest. Different techniques, including fluorescence microscopy, high-performance liquid chromatography, capillary electrophoresis, and spectrophotometry were effectively used for monitoring of species (Cheng et al., 2000; Gong, 2013; Lapainis et al., 2007; Wachman et al., 2004). However, on-site, real monitoring, and selective detection of multi-species in one-post screen assay remain challenge.

Electrochemical biosensors have been gaining significant attention for their capability to recognize biomolecules such as DA, AA, and UA because of their high sensitivity, easy operation, low cost, rapid response, handling convenience, qualification for in situ monitoring, excellent compatibility with miniaturization, and good selectivity (Akhtar et al., 2017; Emran et al., 2017, 2018a, 2018b). DA, AA, and UA coexist in the extracellular fluid of the central nervous system and the serum. A reliable analytical method for the one-pot measurement of DA, AA, and UA levels in a biological sample is urgently needed for the in vitro monitoring of DA from its original sources, including the brain or dopaminergic cells, such as PC12, and even in the human blood serum

* Corresponding author at: National Institute for Materials Science (NIMS), 1-2-1 Sengen, Tsukuba-shi, Ibaraki-ken 305-0047, Japan.
E-mail addresses: sherif.elsafty@nims.go.jp, sherif.el-safty@sunderland.ac.uk (S.A. El-Safty).

https://doi.org/10.1016/j.bios.2018.03.026
Received 15 December 2017; Received in revised form 12 February 2018; Accepted 12 March 2018
Available online 14 March 2018
0956-5663/

(Liu et al., 2014; Qu et al., 2013; Sun et al., 2015a; Wu et al., 2015; Zhang et al., 2013).

The simultaneous detection of DA and UA in the presence of AA was performed based on composite materials (carbon-based materials, such as graphene and multiwall carbon nanotubes and other metal or metal oxides), such as Pt/reduced graphene oxide (Pt/RGO), 3D porous graphene, pDA/(MWCNT), poly(l-methionine)/AuNPs/GCE, 1D carbon nanomaterial, and ZnO-polyaniline/RGO (Ghanbari and Moloudi, 2016; Ojani et al., 2014; Palanisamy et al., 2015; Wang et al., 2016a, 2016b). Previous studies simultaneously detected DA, AA, and UA, such as activated graphene/MWCNT nanocomposite-loaded Au nanoclusters, flexible graphene fiber functionalized by $NiCo_2O_4$ nanowires, Fe_3O_4 @ N-doped carbon nanotubes, Pt@GO, AuNPs-GO poly(2,6-pyridine dicarboxylic acid), N,S-dual doping of porous carbon, CTAB-fGO/MWCNT, NiCo@N-doped carbon nanoplates, and graphene-ZnO (Abdelwahab and Shim, 2015; Cai et al., 2016; Fernandes et al., 2014; Gao et al., 2014; Sun et al., 2011; Tığ et al., 2017; Yang and Li, 2014; Zhang et al., 2015b, 2016). These significant developments of electrodes may enable the simultaneous detection of AA, DA, and UA in on-site monitoring assay. However, fabrication of simple, low-cost capital and easy-to-use electrodes yet associated with high-performance sensing assays of biological target species is urgently needed in future design of electrochemical biosensors for clinical application.

The porous materials has received considerable attention in many applications, such as biosensors, catalysis, fuel cells, antimicrobial, adsorption and energy storage (Aboelmagd et al., 2015; Akhtar et al., 2014; Azzam et al., 2017; Derbalah et al., 2015; El-Safty et al., 2013a; Hassen et al., 2016b; Khairy and El-Safty, 2013, 2014, 2015; Khairy et al., 2012). Carbon-based materials have enormous characteristic features, such as a large surface area, numerous edge-plane-like defects, which are directly reflected on its highly electrocatalytic activity, and significant biosensing applications (Inagaki et al., 2016). The addition of a heteroatoms, such as nitrogen, sulfur, phosphorous, and boron, into the graphitic carbon network could enhance the electrocatalytic activity of carbon materials and change the surface characteristics of the carbon matrix, including hydrophobicity, electrical resistivity, charge transfer, and acid/base levels (Chen et al., 2014; Ismagilov et al., 2009; Xiao et al., 2005).

In the present work, the design of metal-free catalysis electrode based on heteroatom-doped carbon material for the ultrasensitive and selective detection of mono-bioactive molecules in the biological fluids and secreted from living cells was achieved. The S-atoms acted as heteroatom dopants and altered the carbon-microspheres for efficient electrocatalysis with high active sites. The S-MC-1 was characterized and provided a high surface area, a dominant microporous structure, a large pore volume, and a microsphere structure, making it an ideal mediator surface for signaling transduction. The microporous structure with efficient doping of S-atoms created highly efficient active sites, facilitated molecular diffusion, and promoted interactions at electrolyte–electrode interfaces. The S-MC-1 showed a real evidence of selective and simultaneous signaling of AA, DA, and UA in the tertiary mixture. The high biocompatibility, low cytotoxicity, high sensitivity, and significant selectivity of the S-MC-1 were ideal as in vitro DA-sensor model in living cells (PC12) and biological samples.

2. Experimental section

2.1. Synthesis of sulfur-doped microporous carbon (S-MC-1 and S-MC-2)

Sulfur-doped microporous carbon (S-MC) was synthesized as follows: 2 g of D-glucose was dissolved in 50 mL Milli-Q water and sonicated for 30 min. Then, two samples of 0.5 and 1 g of thiourea with a mass ration of D-glucose: thiourea are 4:1 and 2:1. Each one was dissolved in 20 mL Milli-Q water and sonicated for 30 min. The thiourea solution was added to the D-glucose solution and continuously stirred for 4 h. After that, the two solutions were transferred to 100 mL Teflon-sealed autoclaves and maintained at 180 °C for 24 h. After being cooled to room temperature, the black precipitate of the desired materials S-MC-1 (4:1) and S-MC-2 (2:1) were washed several times with water/ethanol and then dried at 60 °C for 24 h. The desired black materials were annealed at 800 °C under N_2 atmosphere for 4 h with a step increase in temperature by 2 °C/min.

2.2. Cell culture

The PC12 cell line was obtained from PC12 (ATCC® CRL1721™) and was cultured by incubation under 5% CO_2 at 37 °C in Dulbecco's Modified Eagle's Medium (DMEM) containing 10% fetal bovine serum (FBS) and 10% heat-inactivated serum. Cells were passaged every five days and the medium was changed two-three times a week throughout the lifetime of all cultures.

3. Results and discussion

3.1. Micrometric spherical construction of S-doped microporous carbon

The spherical construction growth of carbon material was formed with D-glucose acting as the source of carbon spheres after polymerization and carbonization at high temperature under hydrothermal carbonization (HTC) conditions (Wang et al., 2002). The S-doped carbon spheres from D-glucose were formed by adding thiourea as the S-source under hydrothermal conditions. Two different mass ratios of thiourea (% S) was added to 2 g of D-glucose (glucose: thiourea = 4:1 and 2:1) and heated under HTC at 180 °C for 24 h. Aromatization and carbonization were performed with the formation of carbon spheres as in Scheme S1. The presence of thiourea, which is the source of S-atoms during the polymerization and spherical carbon growth, advanced the S-atom to the carbon chain and formed S-doped carbon with different sulfur contents as its source concentration. The complete carbonization of the S-MC was formed with the microporous network after annealing at 800 °C under N_2 flow at an increasing rate of 2 °C/min. After annealing at 800 °C, two varied materials appeared and were named S-MC-1 and S-MC-2 according to the mass ratios of each sample.

3.2. Morphological and structural assessments of S-MC

The S-MC hieratical morphology was investigated through field-emission scanning electron microscopy (FE-SEM), as shown in Fig. S1(A-D). As illustrated in Fig. S1A, a high yield of carbon spheres of S-MC-2 was formed with formally aligned spheres. The formation of spherical carbon from D-glucose was grown after successive condensations and polymerization in a spherical shape. High-magnification FE-SEM resulted in micro-spherical carbon structures with size in the range of 3–5 μm, as presented in the inset of Fig. S1A. Fig. S1B shows that in the low-magnification FE-SEM of S-MC-1, symmetrical and formal micro-spheres of S- doped carbon (S-MC-1) were observed, where a high yield and different spheres size were formed. Fig. S1(C & D) illustrates the formation of spherical carbon with a homogeneous spherical distribution, and 3D spheres construction. The self-assembly of spherical carbon-doped materials was realized with a microsphere structure in the range of 1.5–5 μm.

The effective and actual percentage of S-atoms in the carbon microspheres of S-MC-1 and S-MC-2 were investigated through EDX-SEM. Fig. S1(E-i-E-iv) shows the EDX-SEM for S-MC-1 and displays the homogeneity and formality distribution of the C, O, and S atoms on the sphere's surface. Furthermore, Fig. S1(F-i-F-iv) shows the EDX-SEM for S-MC-2 and displays the presence and distribution of C, O, and S. The % mass for C, O, and S of S-MC-1 and S-MC-2 illustrate the higher percentage for S-atoms in S-MC-2 as thiourea concentration was increased. The mass of S increased from 5.27% of S-MC-1–8.45% of the S-MC-2, whereas the mass of C and O were decreased from 74.1% to 73.07% and from 20.63% to 18.74%, respectively. Thus, the decrease in the mass of

C and O as the S contents were increased may be related to the efficient doping of S-atoms into the carbon chain framework with more edge plane defects.

To investigate the effect of dopant material contents on the graphitic structure nature; Raman spectra were performed for the S-MC constructions. The Raman spectra of all the samples were performed at $\lambda = 532$ nm, a laser power of 4.68 eV, a laser scan of 10 times, and a laser exposure of 10 s in the range of 700–2000 cm^{-1}. Fig. S2A shows two bands at around 1353 and 1563 cm^{-1}, which are characteristic of the D and G bands of carbon materials (Ali et al., 2017; El-Safty et al., 2017; Hassan et al., 2016; Hassen et al., 2016a; Shenashen et al., 2017a, 2016, 2017b). The G band shifted from 1579 cm^{-1} to 1568 cm^{-1} as the % mass of S increased as in S-MC-2. The I_D/I_G values of S-MC-1 and S-MC-2 were 0.93 and 0.95, respectively, illustrating the effects of dopant materials on the graphitic carbon structure. That is, S distorted the graphitic structure and increased the edge plane deficiency, which are reflected in the catalysis, charge transfer, charge density activity.

The surface characteristics, such as the BET surface area, porous structure, and pore volume, of S-MC, were investigated by using N_2 adsorption isotherms. Fig. S2B shows the N_2 adsorption isotherms for S-MC-1 (green line) and S-MC-2 (red line). The adsorption isotherm proceeded similar to a type I isotherm with H4 hysteresis loops, which were related to the formation of microporous constructions (El-Safty, 2008; El-Safty et al., 2015a; El-Safty et al., 2012; El-Sewify et al., 2017; Shenashen et al., 2013a, 2013b, 2014a, 2014b). The S_{BET} of S-MC-1 and S-MC-2 were 522 and 171 m^2g^{-1}, respectively. Fig. S2C and its inset show the NLDF pore distribution for S-MC-1 and S-MC-2, in which the pore size and pore volume of S-MC-1 were 1.52 nm and 0.328 cm^3g^{-1}, whereas those of S-MC-2 were 2.2 nm and 0.1251 cm^3g^{-1}. These results confirmed that the conformation structure was clearly defined as a microporous structure for S-MC-1 and S-MC-2. All of these results proved that S-MC-1 had a high surface area with a microporous structure and a large pore volume (El-Safty et al., 2008, 2015b, 2013; El-Safty and Shenashen, 2013; El-Safty et al., 2015, 2013b; Gomaa et al., 2017; Selim et al., 2018; Soliman et al., 2017).

X-ray diffraction (XRD) analysis revealed the crystalline nature of S-MC-1. As shown in Fig. S2D, two broad peaks were centered at $2\Theta = 29.81^\circ$ and 42°, which were related to graphitic carbon formation (Li et al., 2009). The presence of a broadband at 42° indicated the distortion of the crystalline graphitic carbon and the formation of carbon-doped microspheres. Furthermore, the chemical compositions of the S-MC were investigated by conducting XPS analysis (Fig. S3). The XPS spectra of S-MC showed three peaks centered at 165.1, 531.68, and 284.76 for S, O, and C, respectively (Fig. S3) (for more details, see the Supporting Information).

3.3. Interaction mechanism of DA on S-MC-based electrode

The highly active biosensor for signaling of mono-bioactive molecules, such as AA, DA, and UA, from its resources was successfully assembled. The PC12-cell line was chosen as the neuronal cells model, which can synthesize monoamine neurotransmitters such as DA. The concentration of DA secreted from neuronal cells depends on the concentration of stimulated agents, such as K^+ (Akhtar et al., 2017; Emran et al., 2018a, 2018b). The DA secreted from neuronal cells enriched the PC12 medium and were injected into the electrochemical cell to monitor the DA (Scheme 1). SWV measurements were used to detect DA concentrations with the modified electrode of S-MC-1 as the working electrode. The DA molecules incorporated with the surface of S-MC-1 lead to the enriched electrode surfaces with dense, mobile electron movement along the actively heteroatom S-doped carbon-sphere surfaces. Our finding indicated that the activated of the carbon sphere surfaces with various functional groups such as SO_x, COOH, and OH groups, in addition to the textural surface features such as high surface area, microscopic porous spaces, and spherical networks may lead to highly sensitive and selective sensing of DA released from living cells. Furthermore, the S-MC-1 illustrates an effective catalytic mediation of the selective signaling of mono-bioactive molecules.

3.4. Signaling transduction assessments of S-MC-1 and S-MC-2

The signaling behavior of S-MC-1/GCE, S-MC-2/GCE, and GCE was investigated through cyclic voltammetry (CV), and electrochemical impedance microscopy (Fig. S4). S-MC-1 exhibited the highest electrocatalytic mediator over S-MC-2/GCE and GCE in terms of electron charge transfer, catalytic activity, diffusion pathway, charge resistance, and high active surface electrodes (for more details, see the Supporting Information). Thus, the S-MC-1 displayed a highly active electrochemical mediator, efficient %mass of S-contents, high surface area, and dominant mesoporous structure (Akhtar et al., 2015; Sun et al., 2015b; Yang et al., 2012, 2011).

The electrochemical behavior of mono-bioactive molecules, such as AA, DA, and UA, in the S-MC-1/GCE and S-MC-2/GCE were investigated through CV in 0.1 M PBS (pH 5) at a scan rate of 100 mVs^{-1}. Fig. 1(A&B) shows the catalytic oxidation of 0.5 mM AA and 0.1 mM UA on GCE, S-MC-1/GCE, and S-MC-2/GCE. Irreversible oxidation peaks for AA and UA were observed by shifting the applied potential to negative in the S-MC-1/GCE (0.297 and 0.592 V for AA and UA), S-MC-2/GCE (0.3 and 0. 62 V for AA and UA) and GCE (0.613 and 0.677 V for AA and UA). The S-MC-1/GCE revealed highly catalytic oxidation peaks with an enhanced applied potential peak for more negative, which corresponded to the oxidation of AA to de-hydroxy AA and of UA to quinoid form. The S-MC-1/GCE was a more sensitive electrode than S-MC-2/GCE and GCE for the electrooxidation of AA and UA (Kim et al., 2014; Sheng et al., 2012). The same behavior was observed for 5 μM DA, where the catalytic oxidation current of DA at S-MC-1/GCE (17.88 μA) was higher than that of S-MC-2/GCE (5.88 μA) and GCE (2.5 μA). Furthermore, two significant reversible oxidation-reduction peaks were observed for DA with $\Delta E_{Ox\text{-}Rd} = 53$ mV (Fig. 1C).

The possibility of the simultaneous detection of AA, DA, and UA in one step was investigated by conducting CV on AA (0.5 mM), DA (10 μM), and UA (0.1 mM) in PBS (pH 5) on GCE, S-MC-1/GCE, and S-MC-2/GCE. As shown in Fig. 1D (olive line), a broad peak was observed for all coexisting molecules at the GCE, thus proving the lake efficiency of GCE for the selective signaling of each target. Three well-defined peaks for AA, DA, and UA were observed on S-MC-1/GCE and S-MC-2/GCE. Fig. 1D (wine line) confirmed that

S-MC1/GCE exhibited a significant selective signaling with a higher sensitivity than that of S-MC-2/GCE (Fig. 1D (light blue line)). The E_P peaks on S-MC-1/GCE were at 340, 485, and 650 mV for AA, DA, and UA, respectively, and the ΔE between the oxidation peaks of AA-DA, AA-UA, and DA-UA were 145, 310, and 165 mV, respectively. Thus, The S-MC-1/GCE was suitable for the sensitive and selective detection of AA, DA, and UA in one step.

The pH dependence of the electrocatalytic oxidations of 0.5 mM AA, 1 μM DA, and 0.1 mM UA in the S-MC− 1/GCE were investigated by performing CVs in the pH range of 5–7 at a scan rate of 100 mVs^{-1}. The oxidation peak potentials of the detected biomolecules shifted to negative values within the pH range of 5–7, as shown in Fig. 2(A-D). The peak potentials of AA, DA, and UA with respect to the pH values exhibited linear relationships with the following regression equations: pH = 0.455 − 0.031 E(V) (R^2 = 0.93), pH = 0.87 − 0.072 E(V) (R^2 = 0.964), and pH = 0.1.017 − 0.076 E(V) (R^2 = 0.988) for AA, DA, and UA, respectively (Fig. 2[B, D, F]). The slopes of the straight lines were 0.031, 0.072, and 0.076 for AA, DA, and UA, respectively. These results indicated that the number of number of protons was equal to the number of electrons and further confirmed the suggested mechanism of electrooxidation with the loss of $2e^-/2\,H^+$ (Emran et al., 2017, 2018a, 2018b). Furthermore, the optimum pH solution for the best selective signaling of the mono-bioactive molecules was determined by conducting square wave voltammetry (SWV) in the pH range of 5–7. Fig. S5 and its table illustrate that the applied potential shifted to negative

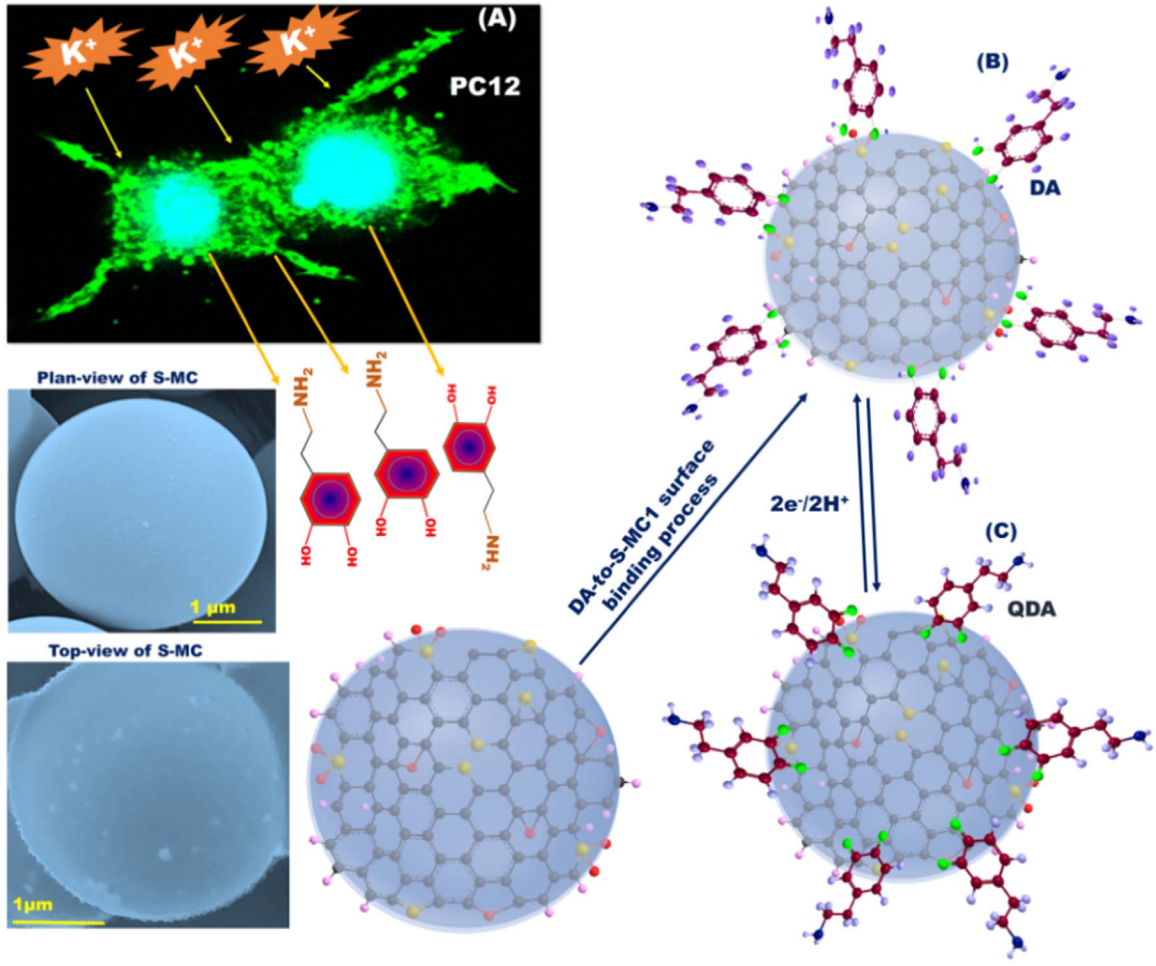

Scheme 1. A) The confocal image of PC12 cells, which synthesize DA under K^+ stimulation. The secreted –DA interact with the surface of S-MC-1, which is constructed from spheres as illustrated from plan and top of view. B) The DA-molecules binds to the active surface of S-MC-1, and then under chemical potential, the DA oxidized to QDA with losing of $2e^-/2H^+$.

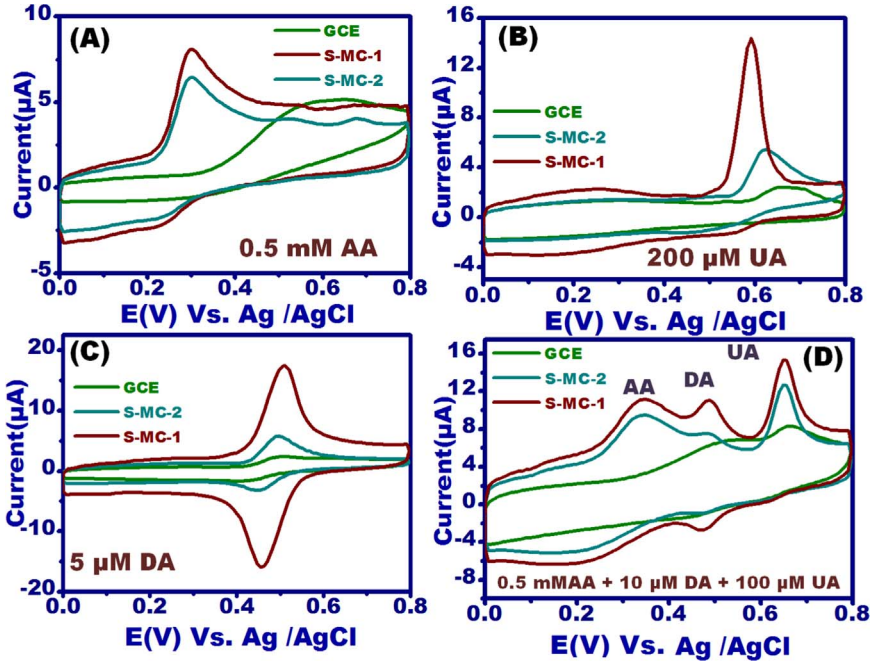

Fig. 1. CVs S-MC-1/GCE (wine line), and S-MC-2 /GCE (light blue line)-modified electrodes and bare GC (olive line) electrode during the detection of 0.5 mM AA (A), 200 μM UA (B), and 5 μM DA (C). D) The simultaneous monitoring of 0.5 mM AA, 10 μM DA and 100 μM UA on GCE (olive line), S-MC-2/GCE (light blue line), and S-MC-1/GCE (wine line) in N_2 saturated of 0.1 M PBS (pH = 5) at scan rate 100 mVs^{-1}.

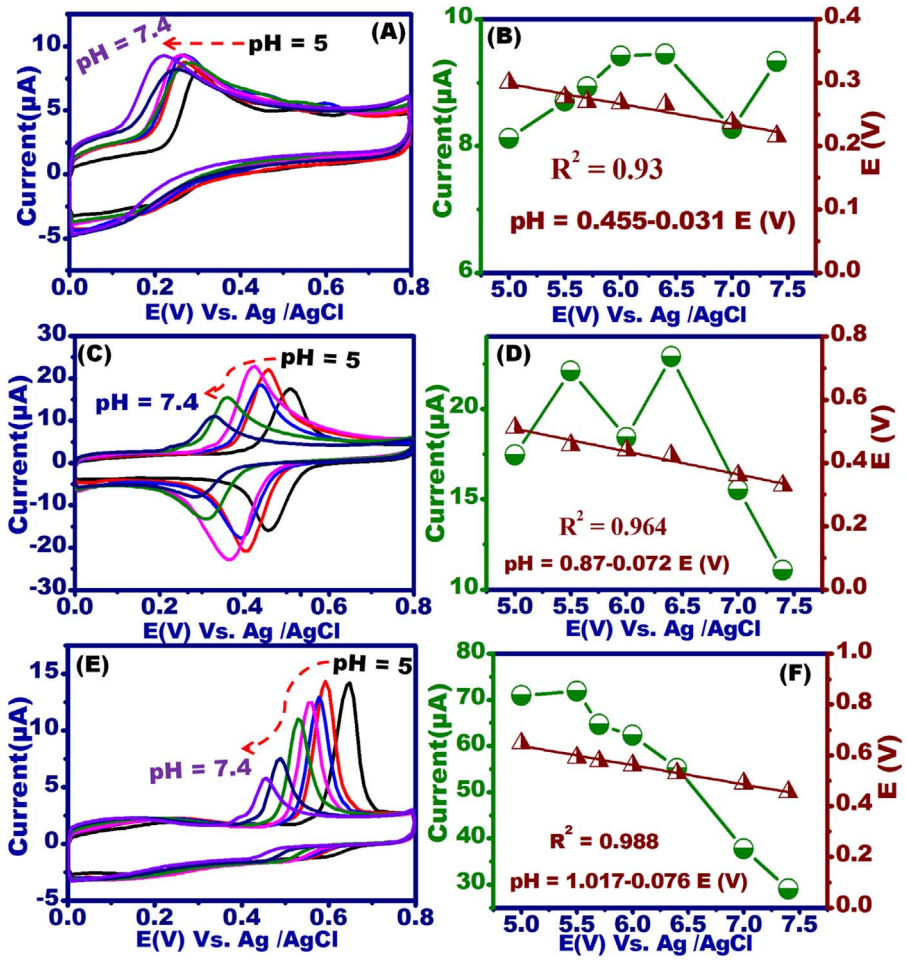

Fig. 2. The CVs of pH-dependent monitoring assay of 0.5 mM AA (A), 1 μM DA, and 100 μM UA using S-MC-1/GCE at different pH ranging from 5 to 7.4 under N_2 saturated of 0.1 M PBS at scan rate 100 mVs^{-1}, and room temperature. The linear-, and scatter-plots of the anodic current (μA) (olive scatter) and applied potential (E(V)) (wine- points) of 0.5 mM AA (A), 1 μM DA, and 100 μM UA using S-MC-1/GCE.

values as the pH values increased. In addition, the best pH supporting electrolyte value was pH 5, at which the highest separation potential values of $\Delta E_{AA\text{-}DA}$, $\Delta E_{AA\text{-}UA}$, and $\Delta E_{DA\text{-}UA}$ were achieved with significant high signals. Thus, pH 5 was used as the optimum pH for the selective signaling of AA, DA, and UA in one step.

The electrochemical kinetics on the surface of S-MC-1/GCE was illustrated by CV at a varying scan rate in 0.1 M PBS (pH 5). The overall process of DA and AA on S-MC-1/GCE was controlled diffusion mechanism, whereas the controlled process of UA was a diffusion-controlled process (for more details, see the Supporting Information, and Fig. S6).

3.5. Monitoring of AA, DA, and UA on S-MC-1

The sensitivity of S-MC-1/GCE for monitoring of AA, DA, and UA was examined through SWV at a frequency of 25 Hz, an amplitude of 25 mV, an integration time of 3 ms, and a step height of 0.5 mV in 0.1 M PBS (pH 5). Fig. 3(A, C & E) shows the SWV oxidation peak current increased with increasing AA, DA, and UA concentrations in the range of 10–4000 μM, 0.01–5 μM, and 1–2000 μM, respectively. Fig. 3A and its inset show the oxidation peak current increased linearly with increasing DA concentrations from 0.01 to 0.1 μM on the S-MC-1/GCE. In addition, the electrode sensitivity of DA decreased because of electrode saturations, which enforced the highest sensitivity of the designed electrode at low DA concentrations. Furthermore, the linear ranges of AA and UA at S-MC-1/GCE are in the range of 10–4000 and 1–2000 μM, respectively (Fig. 3[C&E])). By plotting the concentration versus the current for AA, DA, and UA at low concentrations, a linear relation was obtained with the following regression equations: [I_{DA} (μA) = 1.69 + 154.2 C (μM), R^2 = 0.996, I_{AA} (μA) = 13.22 + 0.038 C (μM), R^2 = 0.964 and I_{UA} (μA) = 3.94 + 0.557 (μM), R^2 = 0.997] (Fig. 3[B, D&F]). The detection limits were found to be 1.26, 0.003, and 0.23 μM (S/N 3) for AA, DA, and UA, respectively. Therefore, S-MC-1/GCE was suitable as a highly sensitive DA sensor with a detection limit of as low as 0.003 μM, which was higher than that of AA and UA by 100–1000-fold, validating that S-MC-1/GCE was an efficient sensitive and selective electrode for biosensing applications.

3.6. Sensitivity and selectivity of AA, DA, and UA on S-MC-1

To demonstrate the sensitivity and selectivity with fine resolution signaling of the mono-bioactive molecules, SWV measurements were performed in 0.1 M PBS (pH 5) on S-MC-1/GCE by varying the concentration of one target while maintaining the concentration of the other two targets constant, and then varying the concentrations of all targets in one-step. Fig. 4A and its inset show that the DA oxidation peak was centered at 0.474 V (vs. Ag/AgCl), and it increased linearly with the addition of DA (0.01–1 μM) in the presence of AA (500 μM) and UA (50 μM). The regression equation is as follows: I (μA) = 6.74 + 100.25 [DA](μM), R^2 = 0.988; N = 3 (Fig. 4B), and the detection limit was calculated to be 27 nM. The DA concentrations higher than 1 μM displayed a nonlinear behavior because of the DA saturation at active adsorption sites. Similarly, the anodic peak currents increased linearly with the concentrations in the range of 20–2000 and 1–400 μM

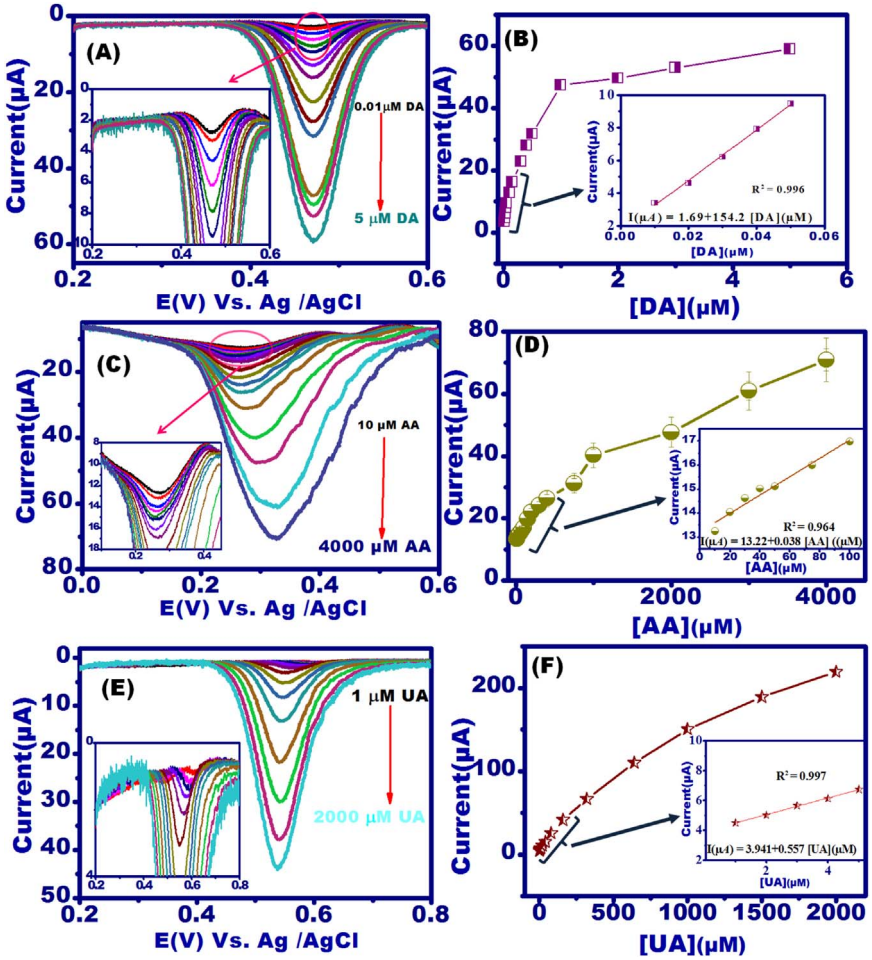

Fig. 3. Square wave voltammetry measurements (SWV) of S-MC-1-modified electrode at varying DA concentrations (0.01–5 μM), its inset the SWV measurements of DA at low concentrations (A), varying the AA-concentrations ranged from 10 to 4000 μM, its inset the SWV measurements of AA at low concentrations (C), and varying the UA-concentrations ranged from 1 to 2000 μM, its inset the SWV measurements of UA at low concentrations (E) in 0.1 M PBS (pH = 5) at step amplitude = 25 mv, frequency = 25 Hz, time of integration = 3 ms and step height = 0.5 mV on S-MC-1/GCE. The calibration plot of AA (B), AA (D), and UA (F)- concentrations (μM) vs the currents (μA), its inset the calibration plot at low concentrations.

for AA (Fig. 4C) and UA (Fig. 4E) in the presence of DA (0.1 μM) and UA (50 μM), and DA (0.05 μM) and AA (400 μM), respectively. The detection limits of AA and UA were determined from the calibration plot of the concentrations vs. the peak currents (Fig. 4(D&F). The regression equations were expressed as I (μA) = 2.08 + 0.35 [AA](μM), R^2 = 0.964 and I (μA) = 4.99 + 0.746 [UA](μM), R^2 = 0.973 for AA and UA with detection limits of 1.9 and 0.8 μM, respectively.

One-step selective signaling with high sensitivity of AA, DA, and UA on S-MC-1/GCE was investigated by SWV. Fig. 4G shows three well-defined peaks at 0.22, 0.422, and 0.57 V, which corresponded to the electrooxidation of AA, DA, and UA at S-MC-1/GCE, respectively. The peak potential separations were up to 200, 178, and 350 mV for AA − DA, DA − UA, and UA − AA, confirming that S-MC-1/GCE can detect AA, DA, and UA in one step. Fig. 4H shows that the SWV anodic current increased linearly with the simultaneous addition of various concentrations of mono-bioactive molecules in the range of 20–200 μM, 0.05–0.35 μM, and 1–10 μM for AA, DA, and UA, respectively. The calibration curves of the simultaneous AA, DA, and UA detection were expressed as I (μA) = 7.53 + 0.0251 [AA](μM); R^2 = 0.88, I (μA) = 3.99 + 83.2 [DA](μM); R^2 = 0.978, I (μA) = 5.74 + 1.04 [UA](μM); R^2 = 0.887, respectively. The calculated detection limits revealed the highest sensitivity and honest selectivity, where the detection limits values were 1.2, 0.0041, and 0.24 μM for AA, DA, and UA, respectively. These findings proved that the S-MC-1-/GCE successfully monitored AA, DA, and UA in one-step with high sensitivity, and selectivity. That is, demonstrate a better performance when compared with other modified electrodes, as presented in Table S1. Furthermore, the S-MC-1/GCE exhibited highly candidate stable sensitive and selective electrode for monitoring of DA in its resources or receptors, such as neuronal cells and human blood.

3.7. One-step detection of AA, DA, and UA in biological sample, monitoring of DA secreted from living cells under K^+- stimulator

The validation of the designed electrode for real application with real human blood serum for the selective screening of bio-interfering molecules (AA, DA, and UA) is summarized in Table S2. The recoveries of the spiked samples were in the range of 100.1–104.3%, 100.8–105%, and 99.84–102.5% for AA, DA, and UA (for more details, see the Supporting Information, and Table S2).

The successful monitoring of neurotransmitter (i.e., DA) levels in the brain and human fluids is urgently needed for the discovery of neurological disorders, such as schizophrenia. The suitability of S-MC-1/GCE for the control in vitro monitoring of DA released from PC12 cells (cells with extracellular DA) was tested (Akhtar et al., 2017; Emran et al., 2018a, 2018b). The PC12 cells were visualized by using laser scanning confocal microscopy measurements after confirming the active wavelength region (Fig. 5A–D). An in vitro model was adopted to study the interaction between S-MC-1 (20 μg/mL) and PC12 cells (2×10^6 cells/mL). DAPI (0.1 μg/mL) was used for PC12 cell nuclear counterstaining, which indicated the localization within the incubated cells (Fig. 5B). Fig. 5A shows the bright field photo of PC12 within S-

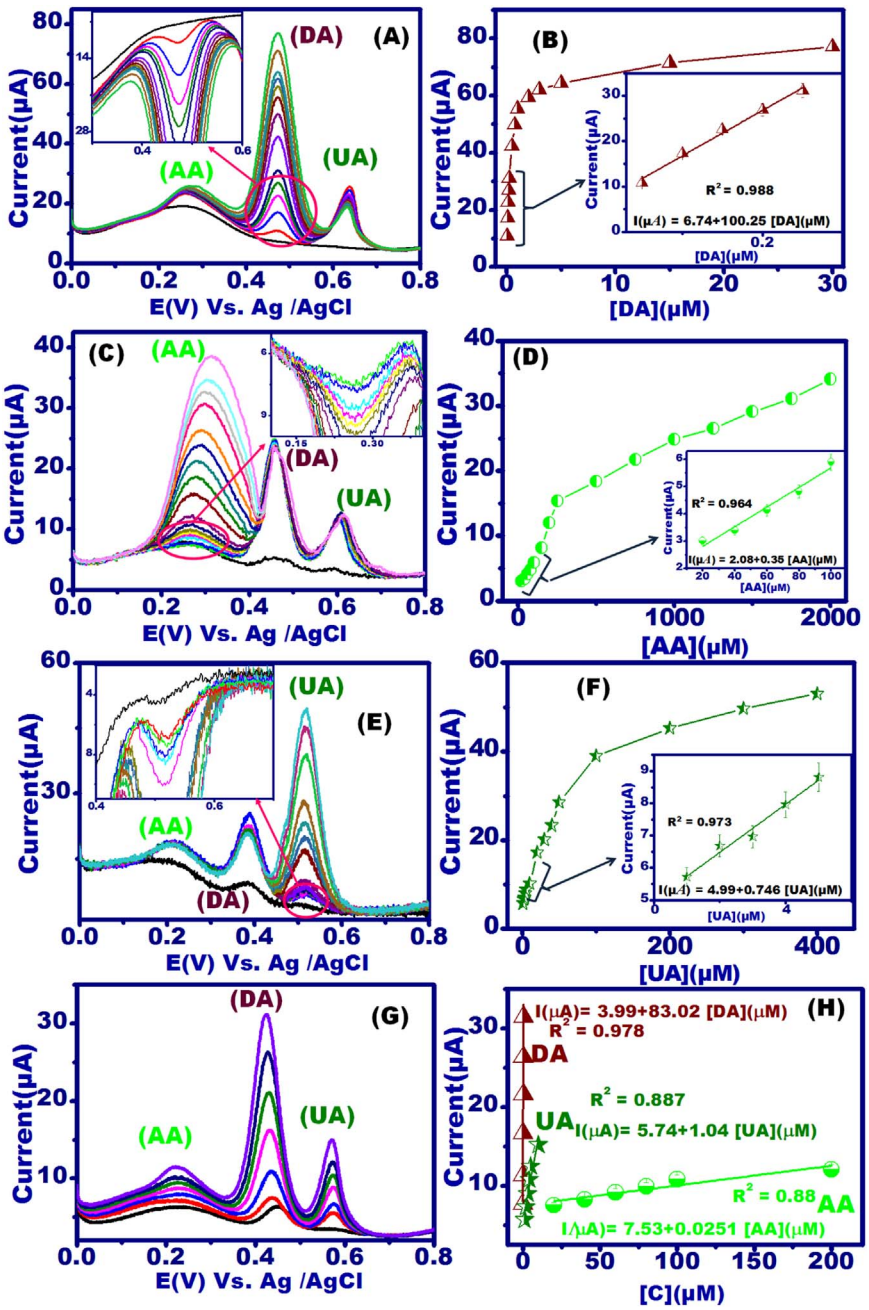

Fig. 4. A) The SWV- measurements of varying DA-concentrations ranged from 0.05 to 30 μM in the presence of 500 μM AA, and 50 μM UA, its inset the SWV measurements of DA at low concentrations. C) SWV of S-MC-1/GCE at varying AA concentrations (20–2000 μM) in the presence of 0.1 μM DA, and 50 μM UA, its inset the SWV measurements of AA low concentrations. E) The SWV-measurements of varying UA-concentrations ranged from 1 to 400 μM in the presence of 0.05 μM DA, and 400 μM AA, its inset the SWV measurements of UA at low concentrations. G) The SWV-measurements of one step adding of AA (20–200 μM), DA (0.05–0.350 μM), and UA (1–10 μM) in 0.1 M PBS (pH = 5) at step amplitude = 25 mv, frequency = 25 Hz, time of integration = 3 ms and step height = 0.5 mV. The calibration plot of DA- (B), AA- (D), and UA- (F) concentrations (μM) vs the currents (μA), its inset the calibration plot at low concentrations. H) The calibration plot of one step adding of AA, DA, and UA-concentrations (μM) vs the currents (μA).

MC-1, where S-MC-1 dispersed and contacted within the cells. Fig. 5(B& C) illustrates the nuclear staining with DAPI (Fig. 5B) and the F-actin staining by phalloidin (Fig. 5C). Fig. 5D shows the merged photo of the nucleus and cytoskeleton of PC12 cells, which indicate the presence of S-MC-1 at the cell membrane without any interference or damage to the cell structure. Thus, S-MC-1 provided high biocompatibility, as it exerted no damage or shrinkage at the cell membrane and no any effect on the nucleus constructions.

The DA released from PC12 cells was monitored through SWV measurements in 0.1 M PBS pH = 5. Fig. S7 shows the SWV measurements of the supernatant of 6×10^6 cells/mL PC12 with and without incubation with different concentrations of (0–75 mM) KCl on S-MC-1/GCE. A sharp well-resolution SWV peak was observed at 0.31 V, which corresponded to the electrooxidation of DA at S-MC-1/GCE. By conducting the calibration curve of DA, each cell will produce 2 nM. Consequently, the effect of the stimulating agent for releasing DA from PC12 was assessed by incubating the PC12 cells with different concentrations of K^+ (25, 50, and 75 mM) for 30 min. As presented in Fig. 5E, the PC12 cells release more DA with increasing concentration of KCl. Furthermore, the results illustrated that the cell membrane was depolarized by K^+ extracellular stimulation and induced an influx of Ca^{2+} and Na^+ by opening the voltage-sensitive Na^+ and Ca^{2+} channels (Mir et al., 2015; Shinohara et al., 2013). In addition, our designed electrode provides high sensitivity and profound highly economic electrode (metal-free-based electrode) that can be employed as DA-sensing in living cells, as shown in Table S3.

To establish an in vitro model for DA-sensing from neuronal cells, the cell proliferation and cytotoxicity of S-MC-1 were investigated by using Cell Counting Kit-8 (CCK-8) assays. The PC12 cells were incubated with S-MC-1 at 37 °C for 24 h with different concentrations of S-MC-1 (10–200 μg/mL). Untreated cells served as a control for all measurements. Fig. 5F shows that 27% of the cells were lost at high concentration of 200 μg/mL and around 8% for 10 μg/mL. Therefore, the S-MC-1 had no significant effect on the cell populations. Thus, the

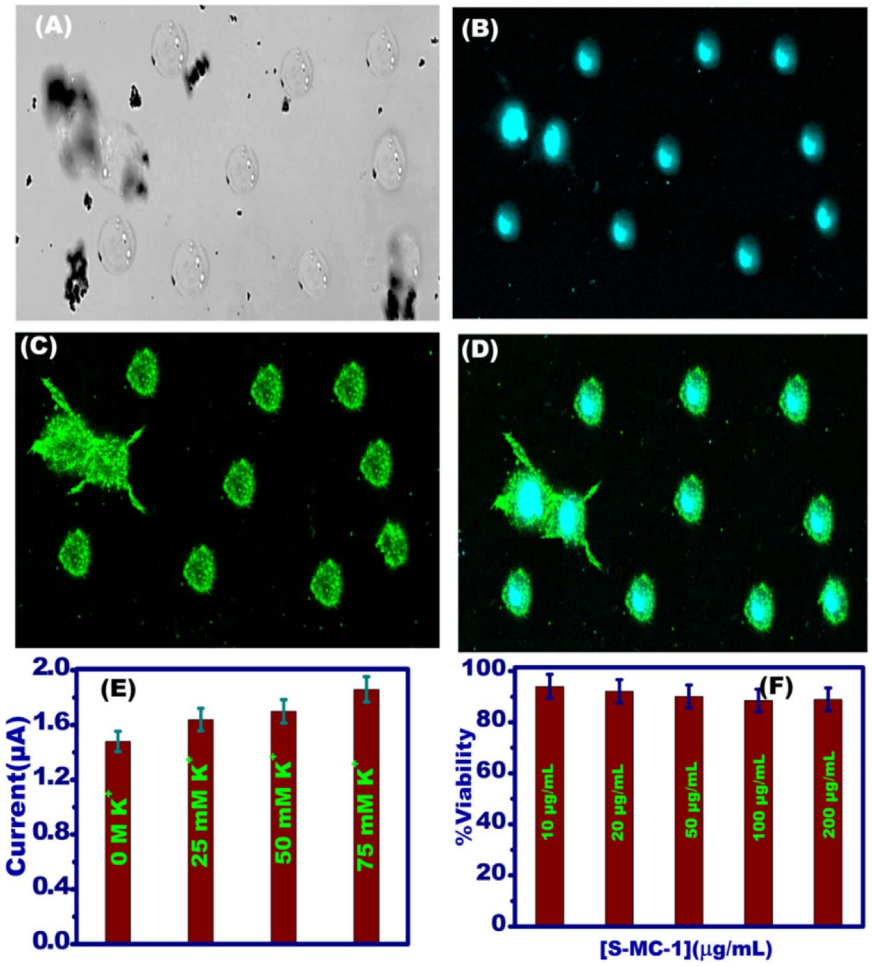

Fig. 5. (A-D) Confocal microscope images recorded at an excitation wavelength of 405, and 488 nm of control PC12 cells. A) Bright field image of S-MC-1incubated with PC12 cells. B) Nucleus blue staining DAPI of the PC12 cells. C) Filamentous actin staining (phalloidin) of the PC12 image. D) Merged image of nucleus and f-actin of PC12. E) The column plot of studying the effect of a stimulating agent of K^+ (0–75 mM K^+) on the amount of DA-secreted from the PC12 using SWV-measurements. F) The cytotoxicity assay of S-MC-1 on the PC12 cell line with various concentrations (10–200 μg/mL) using CCK-8 assay protocol and measured by microplate reader at 450 nm.

cell metabolic activity was too low within the incubation of S-MC-1, verifying its low cytotoxicity.

4. Conclusion

We report a fabrication of simple, low-cost capital and easy-to-use electrodes yet associated with high-performance sensing assays of bioactive AA, DA, and UA molecules using sulfur-doped microporous carbon as an efficient electrochemical biosensor in resources/biological fluid samples. The efficient S-contents resulted in an sp^2-carbon matrix with a high surface area, a microporous structure, which created effectual active sites, and easy molecular diffusion, and facilitated the interactions at electrolyte–electrode interfaces for initiating active signaling transduction. The S-MC exhibited a highly active electrode surface with fast electron-transfer, active signaling of mono-bioactive molecules, facile transduction of electrochemical interaction, and significant selective binding with the targeted molecules. The highly active S-MC-1 achieved selective signaling with high sensitivity and stability, where the detection limits were up to 4.1 nM, 12 μM, and 2.4 μM for DA, AA, and UA for one-step detection, respectively. The S-MC-1 successfully monitored the DA released from dopaminergic cells (PC12) and raised effects of the stimulating agents (K^+) on the amount of extracellular- DA (increasing the extracellular DA secretion). In vitro DA-assay in dopaminergic cells (PC12) was established with high sensitivity, selectivity, biocompatibility, and low cytotoxicity. Our findings proved that the S-MC-1 is a promising material for a highly efficient electrochemical biosensor with high sensitivity, selectivity, and reliable bio-application in human serum for monitoring of mono-bioactive molecules and in vitro DA-sensing in living cells. The S-MC-1 can be employed for routine clinical diagnosis and neuronal investigations.

Acknowledgment

We thank Dr. Miwako Takano, a staff of Young international research center (ICYS), NIMS, 1–2-1 Sengen, Tsukuba 305-0047- Japan, for her assistance in FE-SEM analysis.

Appendix A. Supporting information

Supplementary data associated with this article can be found in the online version at http://dx.doi.org/10.1016/j.bios.2018.03.026.

References

Abdelwahab, A.A., Shim, Y.-B., 2015. Sens. Actuators B 221, 659–665.
Aboelmagd, A., El-Safty, S.A., Shenashen, M.A., Elshehy, E.A., Khairy, M., Sakaic, M., Yamaguchi, H., 2015. Chem. – Asian J. 10 (11), 2467–2478.
Akhtar, N., El-Safty, S.A., Khairy, M., 2014. Chemosensors 2 (4), 235–250.
Akhtar, N., El-Safty, S.A., Khairy, M., El-Said, W.A., 2015. Sens. Actuators B 207, 158–166.
Akhtar, N., Emran, M.Y., Shenashen, M.A., Khalifa, H., Osaka, T., Faheem, A., Homma, T., Kawarada, H., El-Safty, S.A., 2017. J. Mater. Chem. B 5 (39), 7985–7996.
Ali, G.A., Teo, E.Y.L., Aboelazm, E.A., Sadegh, H., Memar, A.O., Shahryari-Ghoshekandi, R., Chong, K.F., 2017. Mater. Chem. Phys. 197, 100–104.

Azzam, A.M., Shenashen, M.A., Selim, M.M., Yamaguchi, H., El-Sewify, I.M., Kawada, S., Alhamid, A.A., El-Safty, S.A., 2017. J. Phys. Chem. Solids 109, 78–88.
Cai, W., Lai, J., Lai, T., Xie, H., Ye, J., 2016. Sens. Actuators B 224, 225–232.
Chen, A., Chatterjee, S., 2013. Nanomaterials based electrochemical sensors for biomedical applications. Chem. Soc. Rev. 42 (12), 5425–5438.
Chen, T., Pan, L., Loh, T., Chua, D., Yao, Y., Chen, Q., Li, D., Qin, W., Sun, Z., 2014. Dalton Transac. 43 (40), 14931–14935.
Cheng, F.-C., Kuo, J.-S., Huang, H.-M., Yang, D.-Y., Wu, T.-F., Tsai, T.-H., 2000. J. Chromatog. A 870 (1), 405–411.
Derbalah, A., El-Safty, S.A., Shenashen, M.A., Abdel Ghany, N.A., 2015. ChemPlusChem 80 (7), 1119–1126.
El-Safty, S.A., 2008. J. Colloid Interface Sci. 319 (2), 477–488.
El-Safty, S.A., Khairy, M., Shenashen, M.A., Elshehy, E., Warkocki, W., Sakai, M., 2015a. Nano Res. 8 (10), 3150–3163.
El-Safty, S.A., Kiyozumi, Y., Hanaoka, T., Mizukami, F., 2008. Appl. Catal. A 337 (2), 121–129.
El-Safty, S.A., Sakai, M., Selim, M.M., Hendi, A.A., 2015b. ACS Appl. Mater. Interfaces 7 (24), 13217–13231.
El-Safty, S.A., Shenashen, M., 2013. Sens. Actuators B 183, 58–70.
El-Safty, S.A., Shenashen, M., Khairy, M., 2013. Colloids Surf. B: Biointerfaces 103, 288–297.
El-Safty, S.A., Shenashen, M.A., Akhtar, N., Selim, M.M., Morsy, W.M., Yamaguchi, H., Kawada, S., Alhamid, A.A., Ohashi, N., Ichinose, I., 2017. Chem. – Asian J. 12 (15), 1952–1964.
El-Safty, S., Abdellatef, S., Ismael, M., Shahat, A., 2013a. Adv. Healthc. Mater. 2 (6), 854–862.
El-Safty, S., Shenashen, M., Ismael, M., Khairy, M., 2012. Adv. Funct. Mater. 22 (14), 3013–3021.
El-Safty, S.A., Sakai, M., Selim, M.M., Alhamid, A.A., 2015. Chem. – Asian J. 10 (9), 1909–1918.
El-Safty, S.A., Shenashen, M., Shahat, A., 2013b. Small 9 (13), 2288–2296.
El-Sewify, I.M., Shenashen, M.A., Shahat, A., Yamaguchi, H., Selim, M.M., Khalil, M.M., El-Safty, S.A., 2017. ChemistrySelect 2 (34), 11083–11090.
Emran, M.Y., Khalifa, H., Gomaa, H., Shenashen, M.A., Akhtar, N., Mekawy, M., Faheem, A., El-Safty, S.A., 2017. Microchim. Acta 184 (11), 4553–4562.
Emran, M.Y., Mekawy, M., Akhtar, N., Shenashen, M.A., EL-Sewify, I.M., Faheem, A., El-Safty, S.A., 2018a. Biosens. Bioelectron. 100, 122–131.
Emran, M.Y., Shenashen, M.A., Mekawy, M., Azzam, A.M., Akhtar, N., Gomaa, H., Selim, M.M., Faheem, A., El-Safty, S.A., 2018b. Sens. Actuators B 259, 114–124.
Farjami, E., Campos, R., Nielsen, J.S., Gothelf, K.V., Kjems, J., Ferapontova, E.E., 2012. Anal. Chem. 85 (1), 121–128.
Fernandes, D.M., Costa, M., Pereira, C., Bachiller-Baeza, B., Rodríguez-Ramos, I., Guerrero-Ruiz, A., Freire, C., 2014. J. Colloid Interface Sci. 432, 207–213.
Gao, W., Feng, X., Zhang, T., Huang, H., Li, J., Song, W., 2014. ACS Appl. Mater. Interfaces 6 (21), 19109–19117.
Ghanbari, K., Moloudi, M., 2016. Anal. Biochem. 512, 91–102.
Gomaa, H.G., Khalifa, H., Selim, M., Shenashen, M.A., Kawada, S., Alamoudi, A.S., Azzam, A., Alhamid, A., El-Safty, S.A., 2017. ACS Sustain. Chem. Eng. 5 (11), 10826–10839.
Gong, J., 2013. New Progress on Graphene Research. InTech.
Hassan, D., El-Safty, S., Khalil, K.A., Dewidar, M., Abu El-Maged, G., 2016. Int. J. Electrochem. Sci. 11, 8374–8390.
Hassen, D., El-Safty, S.A., Tsuchiya, K., Chatterjee, A., Elmarakbi, A., Shenashen, M.A., Sakai, M., 2016a. Sci. Rep. 6, 24330.
Hassen, D., Shenashen, M., El-Safty, S., Selim, M., Isago, H., Elmarakbi, A., El-Safty, A., Yamaguchi, H., 2016b. J. Power Sources 330, 292–303.
Huang, J., Liu, Y., Hou, H., You, T., 2008. Biosens. Bioelectron. 24 (4), 632–637.
Inagaki, M., Toyoda, M., Soneda, Y., Tsujimura, S., Morishita, T., 2016. Carbon 107, 448–473.
Ismagilov, Z.R., Shalagina, A.E., Podyacheva, O.Y., Ischenko, A.V., Kibis, L.S., Boronin, A.I., Chesalov, Y.A., Kochubey, D.I., Romanenko, A.I., Anikeeva, O.B., 2009. Carbon 47 (8), 1922–1929.
Jiang, J., Du, X., 2014. Nanoscale 6 (19), 11303–11309.
Khairy, M., El-Safty, S.A., 2013. RSC Adv. 3 (45), 23801–23809.
Khairy, M., El-Safty, S.A., 2014. Sens. Actuators B 193, 644–652.
Khairy, M., El-Safty, S.A., 2015. J. Energy Chem. 24 (1), 31–38.
Khairy, M., El-Safty, S.A., Ismael, M., Kawarada, H., 2012. Appl. Catal. B 127, 1–10.
Kim, S.-j., Kim, Y.L., Yu, A., Lee, J., Lee, S.C., Lee, C., Kim, M.H., Lee, Y., 2014. Sens. Actuators B196, 480–488.
Lapainis, T., Scanlan, C., Rubakhin, S., Sweedler, J., 2007. Anal. Bioanal. Chem. 387 (1), 97–105.
Li, B.-R., Hsieh, Y.-J., Chen, Y.-X., Chung, Y.-T., Pan, C.-Y., Chen, Y.-T., 2013. J. Am. Chem. Soc. 135 (43), 16034–16037.
Li, X., Zhang, J., Shen, L., Ma, Y., Lei, W., Cui, Q., Zou, G., 2009. Appl. Phys. A 94 (2), 387–392.
Liu, X., Zhu, H., Yang, X., 2014. RSC Adv. 4 (8), 3706–3712.
Mir, T.A., Akhtar, M.H., Gurudatt, N., Kim, J.-I., Choi, C.S., Shim, Y.-B., 2015. Biosens. Bioelectron. 68, 421–428.
Ojani, R., Raoof, J.-B., Maleki, A.A., Safshekan, S., 2014. Chin. J. Catal. 35 (3), 423–429.
Palanisamy, S., Thirumalraj, B., Chen, S.-M., Ali, M.A., Al-Hemaid, F.M., 2015. J. Colloid Interface Sci. 448, 251–256.
Qu, Y., Ma, M., Wang, Z., Zhan, G., Li, B., Wang, X., Fang, H., Zhang, H., Li, C., 2013. Biosens. Bioelectron. 44, 85–88.
Selim, M.S., Elmarakbi, A., Azzam, A.M., Shenashen, M.A., EL-Saeed, A.M., El-Safty, S.A., 2018. Prog. Org. Coat. 116, 21–34.
Shenashen, M., El-Safty, S.A., Khairy, M., 2013a. J. Porous Mater. 20 (4), 679–692.
Shenashen, M., Elshehy, E., El-Safty, S.A., Khairy, M., 2013b. Sep. Purif. Tech. 116, 73–86.
Shenashen, M.A., El-Safty, S.A., Elshehy, E.A., 2014a. Analyst 139 (24), 6393–6405.
Shenashen, M.A., El-Safty, S.A., Elshehy, E.A., 2014b. Part. Part. Syst. Char 31 (3), 293–316.
Shenashen, M.A., Hassen, D., El-Safty, S.A., Isago, H., Elmarakbi, A., Yamaguchi, H., 2017a. Chem. Eng. J. 313, 83–98.
Shenashen, M.A., Hassen, D., El-Safty, S.A., Selim, M.M., Akhtar, N., Chatterjee, A., Elmarakbi, A., 2016. Adv. Mater. Interfaces 3 (24), 1600743.
Shenashen, M.A., Kawada, S., Selim, M.M., Morsy, W.M., Yamaguchi, H., Alhamid, A.A., Ohashi, N., Ichinose, I., El-Safty, S.A., 2017b. Nanoscale 9, 7947–7959.
Sheng, Z.-H., Zheng, X.-Q., Xu, J.-Y., Bao, W.-J., Wang, F.-B., Xia, X.-H., 2012. Biosens. Bioelectron. 34 (1), 125–131.
Shinohara, H., Sakai, Y., Mir, T.A., 2013. Anal. Biochem. 441 (2), 185–189.
Soliman, A.A.E., Shenashen, M.A., El-Sewify, I.M., Taha, G.M., El-Taher, M., Yamaguchi, H., Alamoudi, A.S., Selim, M.M., El-Safty, S.A., 2017. ChemistrySelect 2 (21), 6135–6142.
Sun, C.-L., Lee, H.-H., Yang, J.-M., Wu, C.-C., 2011. Biosens. Bioelectron. 26 (8), 3450–3455.
Sun, J.-y., Gan, T., Deng, Y.-p., Shi, Z.-x., Lv, Z., 2015a. Sens. Actuators B 211, 339–345.
Sun, Y., Wu, J., Tian, J., Jin, C., Yang, R., 2015b. Electrochim. Acta 178, 806–812.
Tığ, G.A., Günendi, G., Pekyardımcı, Ş., 2017. J. Appl. Electrochem. 47 (5), 607–618.
Wachman, E.S., Poage, R.E., Stiles, J.R., Farkas, D.L., Meriney, S.D., 2004. J. Neurosci. 24 (12), 2877–2885.
Wang, C., Li, J., Shi, K., Wang, Q., Zhao, X., Xiong, Z., Zou, X., Wang, Y., 2016a. J. Electroanal. Chem. 770, 56–61.
Wang, Q., Li, H., Chen, L., Huang, X., 2002. Sol. State Ion. 152, 43–50.
Wang, Y., Huang, Y., Wang, B., Fang, T., Chen, J., Liang, C., 2016b. J. Electroanal. Chem. 782, 76–83.
Wu, C., Tang, Y., Wan, C., Liu, H., Wu, K., 2015. Electrochim. Acta 166, 285–292.
Xiao, K., Liu, Y., Hu, Pa, Yu, G., Sun, Y., Zhu, D., 2005. J. Am. Chem. Soc. 127 (24), 8614–8617.
Yang, S., Zhi, L., Tang, K., Feng, X., Maier, J., Müllen, K., 2012. Adv. Funct. Mater. 22 (17), 3634–3640.
Yang, Y.J., Li, W., 2014. Biosens. Bioelectron. 56, 300–306.
Yang, Z., Yao, Z., Li, G., Fang, G., Nie, H., Liu, Z., Zhou, X., Chen, Xa, Huang, S., 2011. ACS Nano 6 (1), 205–211.
Zhang, X., Chen, X., Kai, S., Wang, H.-Y., Yang, J., Wu, F.-G., Chen, Z., 2015a. Anal. Chem. 87 (6), 3360–3365.
Zhang, X., Yan, W., Zhang, J., Li, Y., Tang, W., Xu, Q., 2015b. RSC Adv. 5 (80), 65532–65539.
Zhang, X., Zhang, Y.-C., Ma, L.-X., 2016. Sens. Actuators B 227, 488–496.
Zhang, Y., Gan, T., Wan, C., Wu, K., 2013. Anal. Chim. Acta 764, 53–58.